Ferroelectric control of electron half-metallicity in *A*-type antiferromagnets and its application to nonvolatile memory devices

Peng Jiang [1,2,3] Lili Kang,[1,2] Hua Hao,[1] Xiaohong Zheng,[1,2,*] Zhi Zeng,[1,2] and Stefano Sanvito [3,†]

[1]*Key Laboratory of Materials Physics, Institute of Solid State Physics, HFIPS, Chinese Academy of Sciences, Hefei 230031, China*

[2]*Science Island Branch of Graduate School, University of Science and Technology of China, Hefei 230026, China*

[3]*School of Physics and CRANN Institute, Trinity College, Dublin 2, Dublin, Ireland*

(Received 14 August 2020; revised 3 November 2020; accepted 30 November 2020; published 16 December 2020)

Two-dimensional (2D) *A*-type antiferromagnetic van der Waals (vdW) materials with either intralayer ferromagnetic and/or intralayer antiferromagnetic coupling have sparked great interest due to their potential applications in spintronics. By first-principles design we predict that a heterostructure formed by sandwiching the 2D *A*-type antiferromagnet, 2H-VSe_2, between the 2D out-of-plane ferroelectric, Sc_2CO_2, presents a semimetal band structure with a half-metallic conduction band. The mechanism giving rise to this peculiar structure cooperatively originates from the strong built-in electric field of the double-layer ferroelectric Sc_2CO_2, and from the charge transfer selectively occurring only at one interface. Based on the so-designed Sc_2CO_2/VSe_2 multiferroic heterostructure, two concepts for nonvolatile memory devices are proposed, in which two states ("1" and "0") are realized by switching the polarization direction of the ferroelectric layers. These results demonstrate that the combination of 2D ferroelectrics and *A*-type antiferromagnetic vdW materials provides not only a fascinating way to achieve half-metallicity in 2D materials, but also a route to the design of new types of nonvolatile ferroelectric memory devices.

DOI: 10.1103/PhysRevB.102.245417

I. INTRODUCTION

Half-metallicity, which is characterized by a metallic feature for one spin channel and an insulating feature for the other spin channel, has attracted great interest due to its importance in spintronics [1–10]. It was first discovered in Heusler compounds [11] and later in many other materials, such as manganese perovskites [12], metal-DNA complexes [13], and organometallic benzene-vanadium wire [14], etc. As a result from the rise of 2D materials in the past decade and their great potential in low dimensional spintronic devices, tremendous effort has been made to realize half-metallicity in 2D systems. Overall, 2D half-metal materials can be divided into two categories, namely, intrinsic half-metals (such as iron dihalide [6], transition-metal (TM) dihydride [15], TM dinitride [16], and Cr_3X_4 (X = S, Se,Te) [17]) and other 2D materials tuned to half-metallic by external means (such as transverse electric field [18,19], chemical decoration [20], and carrier doping [21,22]). Since the number of intrinsic half-metals is rather limited, the extrinsic tuning of other 2D materials has proven a very important supplementary way towards 2D half-metals. Especially, half-metals achieved with certain external modulations have the great advantage of easy control over the transition between the half-metallic and the semiconducting state, so that fully spin-polarized current can be switched on and off as necessary, and a typical such example is zigzag-edged graphene nanoribbon (ZGNR) under a transverse electrical field [18]. Consequently, new schemes for realizing half-metallic 2D systems have always been an intriguing topic in spintronics.

It is well known that spin polarization or magnetism is a prerequisite for achieving half-metallicity. Unfortunately, most 2D materials, such as graphene [23], *h*-BN [24], black phosphorus [25,26], etc. [27–30], are not magnetic, a fact that hinders their applications in spintronic devices. In order to solve this problem, various strategies have been proposed to induce magnetism in 2D materials, for example, by defect and decoration engineering [31–34], or by magnetic proximity effect [35,36]. However, none of these schemes appear fully satisfactory. On the one hand, it is difficult to create long-range magnetic ordering between extrinsically introduced local magnetic moments via robust exchange interaction [37]. On the other hand, the substrate-induced magnetic response of 2D materials is also rather limited [38,39]. Consequently, using intrinsic ferromagnetism, originating from the parent 2D lattice, appears more interesting and more practical for device applications.

Very recently, two theoretically predicted 2D materials with intrinsic ferromagnetism, namely, $Cr_2Ge_2Te_6$ [40] and CrI_3 [41], have been successfully synthesized [38,42], paving the way for 2D spintronics at the monolayer level. Unfortunately, the Curie temperatures T_C of both CrI_3 (45 K) and $Cr_2Ge_2Te_6$ (20 K) are much lower than room temperature, even lower than liquid-nitrogen temperature, a fact that greatly limits their practical application in devices. Despite the low T_C, the discovery of such 2D ferromagnets sparkled great interest and inspired the study of novel low-dimensional magnets. An interesting class is that formed by vanadium

*xhzheng@theory.issp.ac.cn
†sanvitos@tcd.ie

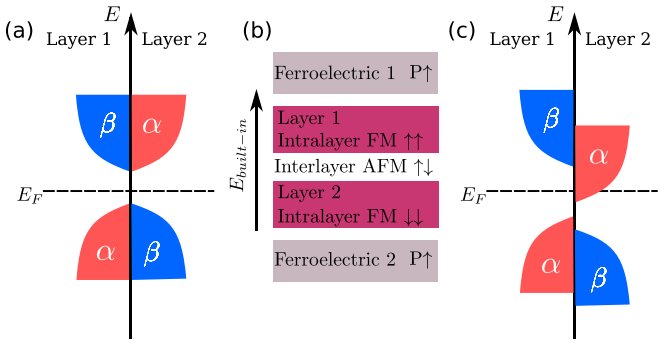

FIG. 1. Schematic illustration of a 2D van der Waals memory. Cartoon of the layer- and spin-resolved density of states of the *A*-type AFM bilayer system (a) without and (c) with stacking a 2D ferroelectric material. Here α and β are the two spin indices for spin up and spin down, respectively. (b) Schematic plot of a vdW multiferroic heterostructure consisting of the *A*-type AFM bilayer crystal sandwiched between two 2D ferroelectric layers. $\uparrow\uparrow$, $\downarrow\downarrow$, and $\uparrow\downarrow$ indicate the magnetic coupling and the magnetization orientation, while P$\uparrow$ is the polarization direction of the ferroelectric layers.

dichalcogenides (VX_2, X = S, Se, Te), which exhibit intrinsic ferromagnetism and high T_C (VS_2: 292 K, VSe_2: 472 K, VTe_2: 553 K), making them promising candidates for room temperature spintronic devices [43–45]. First-principles calculations have revealed that both their 2H and 1T phases are energetically stable [44,46]. More interestingly, bilayer 2H-VSe_2 is an *A*-type van der Waals (vdW) antiferromagnetic (AFM) semiconductor with both ferromagnetic (FM) intralayer coupling and antiferromagnetic interlayer coupling [9,47,48].

Figure 1(a) schematically shows the layer- and spin-resolved density of states for a bilayer *A*-type vdW antiferromagnet. As a conventional antiferromagnet the total density of states is not spin polarized, since the two spin subbands are spin degenerate. In this case, however, the intrinsic ferromagnetism of the monolayers is such that the different spin subbands are spatially located on different monolayers. Based on these features, Gong *et al.* [9] have recently proposed that half-metallicity can be achieved by breaking the symmetry of a VSe_2 bilayer by mean of a vertical electrical field. This provides a mechanism for turning an antiferromagnetic vdW semiconductor into a half-metal. Nevertheless, half-metallicity is achieved at an extremely large critical electric field (40 MV/cm), which is practically a great challenge in the laboratory. Therefore, an interesting question is whether it is possible to achieve half-metallicity in 2H-VSe_2 antiferromagnetic vdW crystals without using an extremely strong external electrical field.

The recent emergence of 2D ferroelectrics provides the possibility of effectively tuning the electronic structures of 2D magnetic materials due to their spontaneous polarization electrical field [49,50]. As for polar systems, the built-in field is generally much larger than any field available in the laboratory by several orders of magnitude. In addition, 2D polar materials have two substantially differently work functions at their two surfaces. Thus, when a 2D polar material is in contact with a 2D nonpolar one, charge transfer arising from the work function mismatch provides a second way for tuning the shift of the band structures. The main idea of this work is to use such a built-in electric field and the different work functions to manipulate the magnetism. Hence, we propose a multiferroic heterostructure that realizes half-metallicity by sandwiching a bilayer *A*-type antiferromagnet between two ferroelectric monolayers with an out-of-plane electrical polarization, as shown in Fig. 1(b). The presence of such a built-in vertical field together with the possible interfacial charge transfer due to the different work functions between different materials is expected to raise the electrostatic potential at the first layer with respect to that at the second one. Consequently, the band energies (density of states) associated with the first layer will be shifted upwards with respect to those of the second layer. This may eventually result in the appearance of states of only one spin at the Fermi level [see Fig. 1(c)]. Note that, for a system to be half-metallic, we can have only the valence band or only the conduction band or both of them of only one spin channel crossing the Fermi level. Figure 1(c) shows a situation where only the conduction band of spin α crosses the Fermi level. In order to demonstrate the feasibility of this proposal we demonstrate, by first-principles calculations, the half-metallicity of a 2H-VSe_2 bilayer sandwiched between two 2D ferroelectric Sc_2CO_2 layers. It is found that, when both the Sc_2CO_2 layers are polarized along the same direction, the so-constructed heterostructure has a semimetal band structure with the valence band located at one of the Sc_2CO_2 layers and the conduction band located at the adjacent VSe_2. Most importantly, the conduction band is fully spin polarized, namely the VSe_2 bilayer is turned into a half-metal. Interestingly, by reversing the polarization of the ferroelectric layers, the 100% spin-polarized state moves to the other VSe_2 layer in the bilayer, and so does the valence band on the adjacent Sc_2CO_2 one. Furthermore, we will show that our proposed vdW heterostructure holds some potential for fabricating new kinds of ferroelectric memory devices.

II. COMPUTATIONAL DETAILS

All geometrical relaxations and electronic structure calculations are performed using the Vienna *ab initio* simulation package (VASP) [51], which is based on density functional theory (DFT) with a plane-wave basis set and the projector-augmented wave method [52]. The exchange and correlation functional is adopted in the generalized gradient approximation (GGA) with the Perdew-Burke-Ernzerhof (PBE) form [53]. The Heyd-Scuseria-Ernzerhof (HSE06) hybrid functional is also adopted for accurately checking the electronic properties of the studied systems [54]. The 2D materials lie in the *xy* plane and along the *z* axis a vacuum region of about 15 Å is introduced to eliminate the interaction between neighboring periodic images. The energy cutoff for the plane-wave basis-set expansion is 500 eV. The convergence tolerance for all the structural optimization calculations is set to 1 meV/Å. The Brillouin zone in the reciprocal space is sampled using a Γ-centered Monkhorst-Pack scheme with $16\times16\times1$ and $21\times21\times1$ k points for structural relaxation and electronic structure calculations, respectively. Dipole corrections are adopted to eliminate the effects due to the spurious electric field along the vacuum direction. In order to fully describe the van der Waals interaction between the layers during the structure relaxation the DFT-D2 method of Grimme

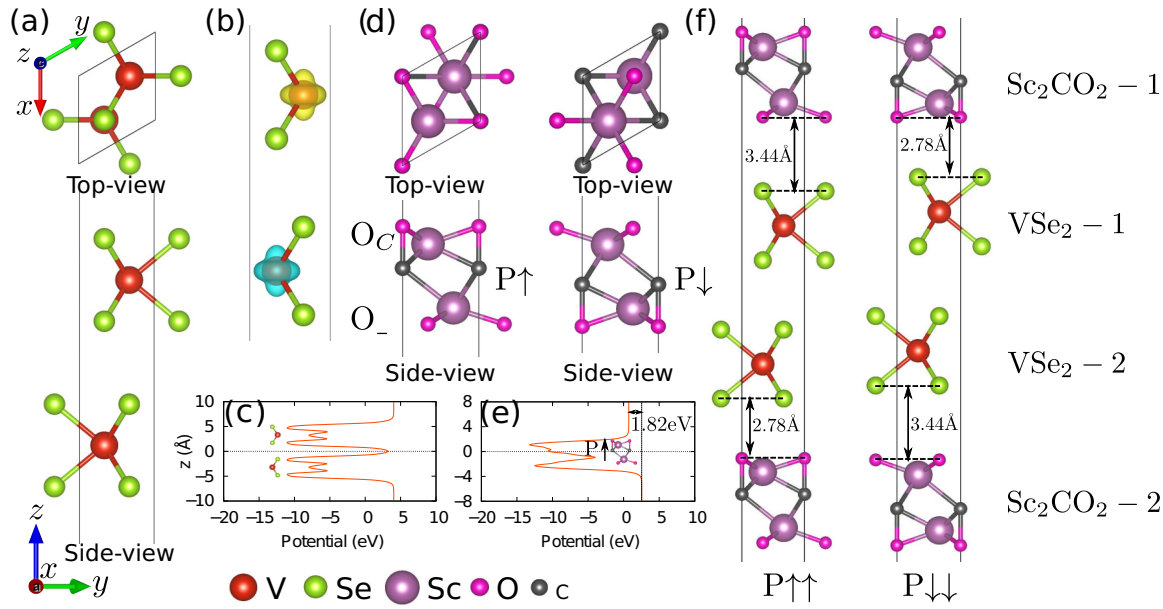

FIG. 2. The structures investigated in this work. (a) Top and side views of the 2H-VSe_2 bilayer. (b) 3D isosurface of the spin density of the 2H-VSe_2 bilayer. The yellow and blue colors denote the spin-up and spin-down components, respectively. (c) The *xy*-planar average of the electrostatic potential of the 2H-VSe_2 bilayer. (d) Top and side views of the 2D ferroelectric material Sc_2CO_2 in the polarized states P↑ and P↓. O_C and O_- are the two oxygen termination planes of the ferroelectric Sc_2CO_2 layer. O_C denotes the side where one C atom is right below each terminating O atom, while O_- denotes the other side. (e) The *xy*-planar average of the electrostatic potentials of a Sc_2CO_2 monolayer. (f) Side view of the 2D vdW multiferroic heterostructure consisting of a bilayer 2H-VSe_2 and two Sc_2CO_2 monolayers with polarization directions pointing both upward (P↑↑) or both downward (P↓↓). VSe_2-1, VSe_2-2, Sc_2CO_2-1, and Sc_2CO_2-2 denote the different VSe_2 and Sc_2CO_2 layers.

is adopted in our calculations [55]. In addition, we take into account on-site correlation in the V 3*d* shell by mean of the GGA + U scheme with on-site Coulomb energy $U = 2.0$ eV and exchange parameter $J = 0.84$ eV, values optimized for the same material in Ref. [9].

III. RESULTS AND DISCUSSION

A. Electronic structures of bilayer VSe_2 and monolayer Sc_2CO_2

We start by investigating the structural and electronic properties of bilayer 2H-VSe_2 (for convenience, it is abbreviated as bi-VSe_2), whose top and side views are shown in Fig. 2(a). The optimized in-plane lattice constant is 3.34 Å and the interlayer distance is 3.22 Å, values that agree well with previous work [9]. Our spin-polarized calculations demonstrate that the *A*-type AFM state with intralayer FM order and interlayer AFM coupling is the ground state of bi-VSe_2, and the spin moment mainly distributes on the vanadium atoms [see the spin density in Fig. 2(b)]. We also calculate the magnetic anisotropy energy (MAE) of the bilayer 2H-VSe_2 with including spin-orbit coupling, which is defined as the energy difference between the magnetization in the out-of-plane (001) and in-plane (100) directions, namely, $E_{\mathrm{MAE}} = E_{001} - E_{100}$. The calculated E_{MAE} is found to be 0.54 meV/f.u., which means that bilayer 2H-VSe_2 is a XY antiferromagnet. This result is consistent with previous investigations [9,44]. The spin-polarized band structures of bi-VSe_2 are then calculated and shown in Figs. 3(a) and 3(b). It is clearly seen that the two spin channels around the Fermi level are degenerate. Interestingly, we find that, in bi-VSe_2, the spin-up states in the valence band are only contributed by the upper VSe_2-1 layer, while the spin-down states in the valence band are only contributed by the bottom VSe_2-2 layer. Likewise, in the conduction band, the spin-up states are only contributed by the bottom VSe_2-2 layer, while the spin-down ones are only contributed by the upper VSe_2-1 layer. This is exactly the situation shown by the cartoon of Fig. 1(a) and it is consistent with previous studies [9].

Based on these unique band features, bi-VSe_2 appears ideal for realizing the proposal of Son *et al.* of electrically tuning the magnetic state towards half-metallicity [9,18]. However, just as indicated by Kan *et al.* [56], the electric field required for generating half-metallicity in such schemes is typically too strong and thus not practical. Instead, we propose here an alternative and probably a more feasible strategy. We sandwich bi-VSe_2 between two monolayers of a 2D ferroelectric material with out-of-plane spontaneous polarization. This will introduce a built-in potential gradient that will play the same role of an external field to introduce a potential energy difference between different layers along the vertical direction.

Recently, many 2D ferroelectric materials with in-plane polarization, such as monolayer black phosphorous-like Group IV chalcogenides MX (M = Ge, Sn; X = S, Se, Te) [57–60], or with out-of plane polarization, such as III_2-VI_3 compounds [61–64], MXene Sc_2CO_2 [65], $Hf_2VC_2F_2$ [66], and $MoTe_2$ [67], have been theoretically proposed. Some of them have been also experimentally fabricated such as In_2Se_3 [62,64] and $MoTe_2$ [67]. Here we take MXene Sc_2CO_2 to building the vdW multiferroic heterostructure displayed in Fig. 2(d). Sc_2CO_2 possesses an intrinsic out-of-plane

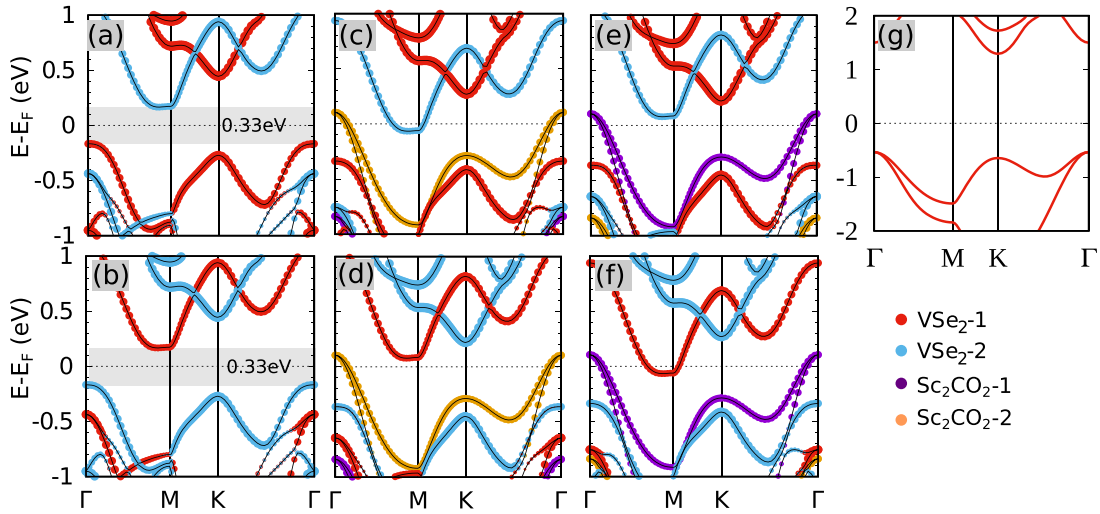

FIG. 3. The layer- and spin-resolved band structures for: (a) spin up of the free-standing VSe_2 bilayer; (b) spin down of the free-standing VSe_2 bilayer; (c) spin up of the Sc_2CO_2/VSe_2 system in the P↑↑ state; (d) spin down of the Sc_2CO_2/VSe_2 system in the P↑↑ state; (e) spin up of the Sc_2CO_2/VSe_2 system in the P↓↓ state; and (f) spin down of the Sc_2CO_2/VSe_2 system in the P↓↓ state. The different colors represent the contributions from the different layers in the heterostructure. (g) The band structure of a single layer of Sc_2CO_2.

polarization and good lattice matching with bi-VSe_2. The optimized lattice constant of monolayer Sc_2CO_2 is 3.44 Å, which means a very small lattice mismatch (3.0%) with bi-VSe_2 (3.34 Å). The band structure of Sc_2CO_2 is shown in Fig. 3(g). It is that of a wide-gap insulator with a GGA + U indirect band gap of 1.83 eV.

B. Electronic structure of the Sc_2CO_2/VSe_2 multiferroic heterostructure

In our proposed structure bi-2H-VSe_2 is stacked vertically between two Sc_2CO_2 monolayers to form a multiferroic vdW heterostructure. Here we consider two different polar configurations, in which the polarization directions of the two ferroelectric layers are either both pointing upward (denoted as P↑↑) or both downward (denoted as P↓↓), as shown in Fig. 2(f). Switching between these two states can be driven by a uniform vertical electric field pulse. When constructing the heterostructure a slight compressive strain is exerted on Sc_2CO_2 in order to match the in-plane lattice constant of VSe_2 (3.34 Å). After structural relaxation, it is found that the interlayer distance between VSe_2 and the O_ termination of Sc_2CO_2 is 3.44 Å, while that with the O_C termination is 2.78 Å for both the P↑↑ and P↓↓ configurations. In addition, we also calculate the energy difference of bilayer VSe_2 between FM and AFM states in the proposed Sc_2CO_2/VSe_2 heterostructure and find that $E_{FM} - E_{AFM} = 0.8$ meV/f.u., which is slightly smaller than $E_{FM} - E_{AFM} = 1.0$ meV/f.u. in the pristine bilayer VSe_2. This means that the whole sandwich heterostructure still favors antiparallel magnetic coupling between interlayers. In order to determinate the stability of the proposed multiferroic heterostructure, its binding energy per unit area E_b is calculated as $-89\,\text{meV/Å}^2$, demonstrating that Sc_2CO_2/VSe_2 is a typical vdW heterostructure. We define $E_b = (E_{\text{heter}} - E_{VSe_2} - 2E_{FE})/2S$, where E_{FE}, E_{VSe_2}, and E_{heter} are the total energy of the individual Sc_2CO_2, VSe_2, and Sc_2CO_2/VSe_2 vdW multiferroic heterostructure, respectively, and $2S$ denotes two contact areas between two Sc_2CO_2 layers and bilayer VSe_2 in the heterostructure. As expected, the negative binding energy demonstrates the stability of the structure and the feasibility of experimentally forming Sc_2CO_2/VSe_2 vdW multiferroic heterostructures. Note that the binding energy at the Sc_2CO_2/VSe_2 interface is about $-76\,\text{meV/Å}^2$, since the elastic energy cost associated with strain Sc_2CO_2 is $13\,\text{meV/Å}^2$. This binding energy value is slightly larger than what is typically found in conventional 2D heterostructures, suggesting that there may be contributions to the binding interaction additional to van der Waals only [68]. This will be discussed later on in relation to the interlayer charge transfer. We have also calculated the MAE of the Sc_2CO_2/VSe_2 heterostructure and obtained an E_{MAE} of about 0.33 meV/f.u. This is slightly smaller than that of the free-standing bilayer 2H-VSe_2, meaning that the easy magnetization axis is still along the in-plane direction.

Next, in order to investigate the influence of the ferroelectric polarization on the electronic structure of bi-VSe_2, we calculate the spin- and layer-resolved band structures of the Sc_2CO_2/VSe_2 heterostructure with either the P↑↑ or the P↓↓ polarization configuration. These are shown in Figs. 3(c)–3(f). Looking at the P↑↑ case [see Figs. 3(c) and 3(d)] it is found that the presence of the ferroelectric layers induces an insulator-to-metal transition. The Fermi level cuts through the valence band of the bottom Sc_2CO_2-2 layer, while it remains in the band gap associated with the upper Sc_2CO_2-1 one. The presence of holes in the heterostructure is compensated by an electron pocket associated with the VSe_2 bilayer. This is fully spin polarized and the band at the Fermi energy is completely dominated by spin-up states. The electronic structure is thus that of a semimetal with a fully spin-polarized conduction band. Given the spatial separation of the electron and hole pockets, the VSe_2 bilayer has the electronic structure of an electron half-metal.

By reversing the direction of the electrical polarization of the ferroelectric layers, as shown in Figs. 3(e) and 3(f), we

find that the bilayer VSe_2 remains half-metallic. However, now only spin-down states cross the Fermi level and they are fully localized on the upper VSe_2-1 layer. At the same time the valence band is now associated with the upper Sc_2CO_2-1 layer, namely it remains localized on the Sc_2CO_2 layer adjacent to that of bi-VSe_2 sustaining the metallicity. In addition, it is important to note that, regardless of the polar configuration, the layer-resolved bands of the individual VSe_2 and Sc_2CO_2 layers resemble extremely closely those of the isolated monolayers. This indicates that there is nearly no band hybridization, but only a relative band shift in the heterostructure. It is well known that the PBE or PBE + U functional generally cannot describe correctly the band feature of the system. Thus we have also performed HSE06 hybrid functional calculations to check the results and found that the band gap of the 2H-VSe_2 bilayer is 1.01 eV, well consistent with the previous study [9]. Figure S1 in the Supplemental Material (SM) presents the layer-resolved and spin-resolved density of states (DOS) of the P↑↑ and P↓↓ configurations [69]. It is found that, in the P↑↑ (P↓↓) configuration, the bottom (upper) Sc_2CO_2 layer exhibits metallic behavior. Moreover, half-metallicity can be observed in the bilayer VSe_2 and the fully spin-polarized states are located on the bottom (upper) one, which is in good agreement with the results obtained with the PBE + U functional. It is also important to note that the energy difference between P↑↑ and P↓↓ is zero. In spite of this, these two states will be very stable and the switch between them can only be achieved by an electrical field to reverse the ferroelectric polarization direction. Thus, they are two bistable states. These results indicate that the construction of a vdW heterostructure using 2D ferroelectric materials is an effective way to tune the half-metallicity of the A-type antiferromagnetic crystal bi-VSe_2.

C. Electrostatic potential distribution and interfacial charge transfer analysis

In what follows we will discuss the physics behind the ferroelectric control of the half-metallicity in the Sc_2CO_2/VSe_2 heterostructure. The electrostatic potential $V(x, y, z)$ across the structure is studied and $\bar{V}(z) = \int V(x, y, z)dxdy/N_xN_y$, its average over the x-y plane, is shown as a function of z, in Fig. 2(c) for bi-VSe_2 and in Fig. 2(e) for Sc_2CO_2. It is seen that the electrostatic potential at the upper and lower VSe_2 layer is identical. Compared to the 2D system, VSe_2, the averaged electrostatic potential of the ferroelectric Sc_2CO_2, differs significantly. In particular, the potential difference between the two sides of bi-VSe_2 is zero [see Fig. 2(c)], while that of Sc_2CO_2 is as large as 1.82 eV [see Fig. 2(e)]. This means that the work function will differ by 1.82 eV on the two sides of Sc_2CO_2. Thus, there emerges a built-in electric field in Sc_2CO_2 due to its broken structural centrosymmetry and the out-of-plane ferroelectric polarization [49,65]. When two layers of Sc_2CO_2 are put in parallel, namely when their ferroelectric polarization vectors point in the same direction, just as in the P↑↑ case, their dipole fields will add up and produce an electrostatic potential difference, and the associated built-in electric field, along the z axis [see the right inset in Fig. 4(a)]. Such a built-in electric field will act upon the sandwiched bi-VSe_2. In order to demonstrate the effect of such potential

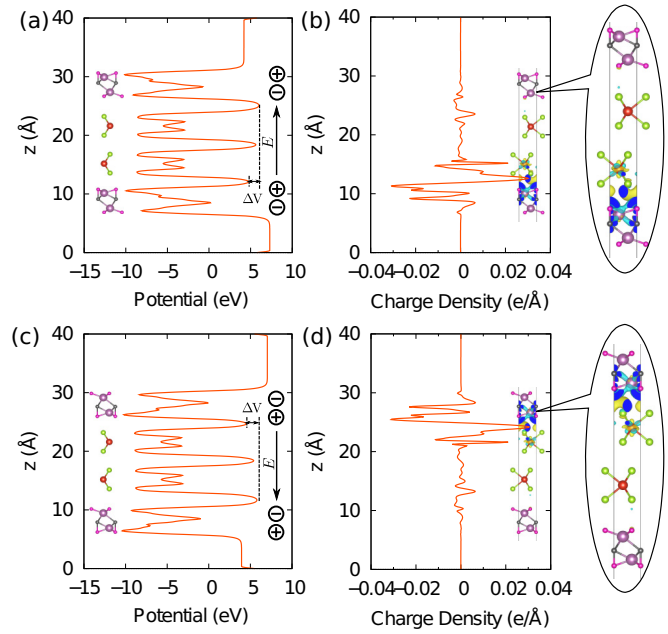

FIG. 4. Planar average electrostatic potential along the z axis in the (a) P↑↑ and (c) P↓↓ configurations. Planar average differential charge density along the z axis in the (b) P↑↑ and (d) P↓↓ configurations. The insets in (b) and (d) show the real-space differential charge density in the P↑↑ and P↓↓ configurations.

difference, the averaged electrostatic potential energy over the x-y plane along the z axis is shown in Fig. 4(a). It is clearly observed that the potential energy at the bottom VSe_2-2 layer is lower than that in the upper VSe_2-1 one. In particular, there is a potential energy difference ΔV (the difference between the minimum of the electrostatic potential at the two interfaces O_- and O_C) of about 1.28 eV between the two VSe_2 layers, which results in the spin splitting. This is in good agreement with the band structures shown in Fig. 3(c), where we observe the conduction band minimum (CBM) of VSe_2-2 below the Fermi level while that of VSe_2-1 above it. The P↓↓ case is equal and opposite to that of P↑↑ [see Figs. 3(e), 3(f) and 4(b)].

Although the discussion so far explains in detail the electrostatics of the problem, in order to understand the peculiar band structure we need to investigate further the charge transfer taking place in the heterostructure. The 3D differential charge density and the corresponding planar average over the x-y plane along the z direction for both the P↑↑ and P↓↓ cases are shown in Figs. 4(b) and 4(d). We observe that the charge transfer is always localized at the VSe_2-Sc_2CO_2 interface with interlayer distance of 2.78 Å, where the VSe_2 faces the O_C termination plane of Sc_2CO_2. In contrast, at the 3.44 Å-separated interface, where VSe_2 faces the the O_- termination plane of Sc_2CO_2, the charge transfer is negligible, regardless of the polarization direction. In order to understand this feature, we have calculated the work functions of Sc_2CO_2 and VSe_2. For a 2D polar system the work functions measured at the two sides of the material is different. Thus, one calculates two work functions for the ferroelectric Sc_2CO_2 layer, namely, $W_1 = 3.42$ eV for the O_C surface and $W_2 = 5.24$ eV for the O_- one. For the nonpolar VSe_2, we have a single value

of $W = 5.37$ eV. It is clear that W and W_2 are very close, thus that charge transfer between the VSe_2 layer and the O_- surface results to be negligible. However, W is much larger than W_1, so that it is much easier for electrons to transfer through the O_C surface of Sc_2CO_2 to the VSe_2 layer. This makes the valence-band maximum (VBM) of Sc_2CO_2-2 partially empty and the CBM of VSe_2-2 partially occupied in the P↑↑ case. In contrast, since there is no charge transfer at the interface between Sc_2CO_2-1 and VSe_2-1, the CBM of VSe_2-1 remains empty, which is fully consistent with the band structures of Figs. 3(c) and 3(d).

Consequently, both the polarization-induced built-in field and the charge transfer, promoted by the work function mismatch, mutually contribute to reinforce the band shift. However, we have to note that [see Fig. S1 and Figs. 3(c)–3(f)] the spin splitting of the VBM is much smaller than that of the CBM in the VSe_2 layers. Notably, the valence band of VSe_2 is always fully filled, so that its associated shift is not due to the interfacial charge transfer, but mainly to the built-in polarization field. In contrast, the conduction band of VSe_2 becomes partially filled due to charge transfer and its spin splitting is much larger. Thus, interfacial charge transfer plays the major role in the spin splitting. This feature makes the spin splitting of the valence band much smaller than that of the conduction band for our ferroelectric sandwich structure and, as a result, the half-metallicity is solely attributed to the conduction band. In comparison, when an external electric field is applied [9], the valence and conduction energy states are shifted towards the opposite direction, so that the band shifts in the valence and the conduction band are comparable, with both bands contributing to the half-metallicity. This is because states belonging to different bands are spatially placed over two different layers along the field direction.

The charge transfer also explains well why the interface with O_C termination has the shorter interface distance of 2.78 Å when compared to that with O_- termination (3.44 Å). Take the P↑↑ case as an example. In the lower interface with O_C termination, after charge transfer the Sc_2CO_2-2 layer remains positively charged while VSe_2-2 is negatively charged. The attractive Coulomb interaction between these two layers greatly decreases their layer distance. On the contrary, due to the negligible charge transfer between Sc_2CO_2-1 and VSe_2-1 at the upper interface and consequently the absence of a strong attractive Coulomb interaction, the layer distance between them is much longer, namely it remains the one determined by the dispersive interactions. With a similar analysis, we can understand the change in charge transfer and the interface distance for the other polarization configuration.

D. Ferroelectric memory device based on Sc_2CO_2/VSe_2 heterostructure

Next, we suggest that the Sc_2CO_2/VSe_2 vdW heterostructure is not only capable of producing half-metallic transport, but it is also a promising structure for designing new kinds of ferroelectric memory devices. In the following we propose two prototypes of memory devices. Device 1 [see Fig. 5(a)] uses the Sc_2CO_2 layer as source/drain metallic contact and the bilayer VSe_2 as channel. The junction can be prepared in two ferroelectric configurations. In the parallel (P) configuration

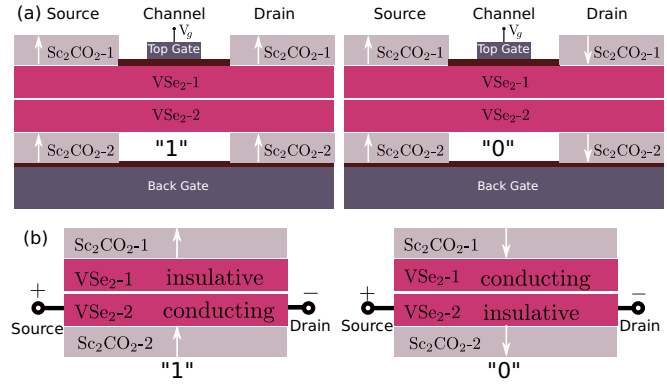

FIG. 5. Two prototypes of ferroelectric nonvolatile memory devices based on the Sc_2CO_2/VSe_2 vdW heterostructure. In (a) device 1 the Sc_2CO_2 layers act as source/drain contacts and bi-VSe_2 as channel. In (b) device 2 only one VSe_2 is electrically contacted and the Sc_2CO_2 layers provide electrostatic gating.

both leads are arranged as P↑↑, while in the antiparallel (AP) one the left lead is P↑↑ and the right lead is P↓↓. In the P configuration the bottom Sc_2CO_2-2 and VSe_2-2 layers exhibit metallicity, while the upper Sc_2CO_2-1 and VSe_2-1 ones behave as a semiconductor, as indicated by the band structure of Figs. 3(c) and 3(d), for both the left-hand and right-hand side leads. Thus electrons injected from the metal lead will move from the left-hand side to the other side through an intralayer VSe_2-2 path. For simplicity, we denote this state as "ON" or "1" state. In contrast, in the AP configuration, obtained by reversing the ferroelectric polarization of the right-hand side lead to P↓↓ with an electric-field pulse, in the right-hand side lead the upper Sc_2CO_2-1 and VSe_2-1 layers are conducting while the bottom Sc_2CO_2-2 and VSe_2-2 layers are insulating. Then, in the left-hand side lead the upper Sc_2CO_2-1 and VSe_2-1 layers are insulating, while the bottom Sc_2CO_2-2 and VSe_2-2 are conducting. In this configuration the conduction path involves electrons hopping from VSe_2-2 on the left-hand side to VSe_2-1 on the right-hand side. This process, however, is highly suppressed due to spin mismatch, since the transport in the two VSe_2 layers is fully spin polarized with opposite spin polarization. In this sense the induced half-metallicity of bi-VSe_2 is the electronic feature giving rise to a potentially huge tunnel electroresistance (TER) in the device. The AP configuration is thus the "OFF" or "0" state of the device. Note that the OFF state in practice will not correspond to an infinite resistance due to unavoidable spin-flip scattering.

In device 2 the two metallic leads are connected with only one of the VSe_2 layers [VSe_2-2 in the case of Fig. 5(b)]. When the entire device is in the P↑↑ configuration, electrons can propagate through VSe_2-2 (1 state). In contrast, when the junction is driven into the P↓↓ configuration by an external electrical-field pulse, electron transmission will be completely blocked in VSe_2-2 but possible in VSe_2-1. Thus, P↓↓ will correspond to the 0 state. In both schemes, the polarization state of the ferroelectric Sc_2CO_2 layers is converted into and detected by the conducting state of the VSe_2 in the data reading process.

The key to realizing the unique function of the proposed devices is how to switch the polarization by applying an

external electric field in a semimetallic system. However, unlike semiconducting or insulating ferroelectrics, switching the polarization is difficult in a ferroelectric (semi)metal due to its relatively high free-charge concentration. In fact, an applied bias induces electrical current rather than acts on the polar distortion. Nonetheless, the flow of the electrical current can be prevented by insertion of a dielectric layer, thus it is possible to apply an electric field to the Sc_2CO_2/VSe_2 heterostructure and realize electric polarization switching. This approach has been successfully applied in ferroelectric semimetal WTe_2 [70]. Moreover, note also that typically in 2D materials the *c*-axis mobility (across the layers) is orders of magnitude smaller than the in-plane one, which is beneficial for the reverse of ferroelectric polarization under an electrical field. In addition, the electric polarization switching of Sc_2CO_2 is reported to involve a multistep process of oxygen and carbon atoms displacements through an intermediate antiferroelectric (AF) structure. Thus, it is necessary to consider an AF heterostructure (APH) shown in Fig. S2 in the SM [69]. We have calculated the total energy of such APH configuration and found that the total energy of the antiferroelectric heterostructure is 433 meV/f.u. higher than those of the proposed P↑↑ and P↓↓ multiferroic heterostructures, which demonstrates that P↑↑ and P↓↓ are the most stable.

Finally, we extend to discuss the effect of monolayer Sc_2CO_2 on the electronic structure of bi-VSe_2. We have calculated the spin- and layer-polarized band structures of the Sc_2CO_2/VSe_2 heterostructures with monolayer Sc_2CO_2 contacted at only one side of bi-VSe_2, and the calculated results are shown in Fig. S3 in the SM [69]. When bi-VSe_2 is in contact with O_- termination plane of Sc_2CO_2, namely, P↑ configuration, both Sc_2CO_2 and bi-VSe_2 still retain their own intrinsic semiconducting characters. There is no charge transfer between Sc_2CO_2 and bi-VSe_2. When the polarization state of monolayer Sc_2CO_2 is reversed, namely, P↓ configuration, half-metallicity can be observed in bi-VSe_2 and the fully spin-polarized states are located at the upper layer (VSe_2-1), which results from the fact that the partial electrons in Sc_2CO_2 are transferred into the VSe_2-1 layer. From this result it appears that the geometry having only one Sc_2CO_2 layer in contact to the VSe_2 bilayer provides another valuable scheme to achieve half-metallicity in VSe_2. The difference between using one or two Sc_2CO_2 layers is that, in the one-layer case, half-metallicity is only obtained in the VSe_2 layer closer to Sc_2CO_2 and the spin polarity of the carriers cannot be changed. In contrast, with the double-layer structure, both the spatial layer distribution of the half-metallic states and their spin polarity can be switched upon reversing the ferroelectric polarization of Sc_2CO_2. This provides an additional degree of freedom for the electrical control of the magnetism and the transport properties of our nanostructure.

IV. SUMMARY

In summary, we have designed a vdW multiferroic heterostructure by sandwiching a bilayer *A*-type antiferromagnetic 2D material VSe_2 between two layers of 2D ferroelectric Sc_2CO_2. By using density functional theory, we have shown that the VSe_2 bilayer exhibits half-metallicity, with the fully spin-polarized state being localized at one layer of the bilayer, and the entire structure presenting a semimetal band structure. Changing the ferroelectric polarization of Sc_2CO_2 reverses both the spin polarity and the spatial localization of the half-metallic state. The working mechanism of the heterostructure is well explained by the polarization-induced built-in electric field and by the associated charge transfer. Such vdW multiferroic heterostructure can be employed not only for generating highly spin-polarized currents, one of the goals of the field of spintronics, but also for realizing new kinds of ferroelectric memory devices. A conventional ferroelectric tunnel junction uses a ferroelectric thin film as tunnel barrier and it works on the principle that changing the direction of the electric polarization changes the tunnel barrier electrostatic profile [71–73]. Our work proposes a totally new design, where the conducting state of bi-VSe_2 is controlled/switched by manipulating the electrical polarization of Sc_2CO_2. We note that the heterostructure investigated here is just one of the possible examples combining half-metallicity and ferroelectricity in 2D. We expect that additional structures implementing the same concept can be proposed and eventually fabricated.

ACKNOWLEDGMENTS

X.Z. acknowledges financial support by the National Natural Science Foundation of China (Grant No. 11974355). S.S. thanks the Irish Research Council (IRCLA/2019/127) for financial support. P.J. thanks the China Scholarship Council (No. 201906340057) for financial support. Calculations were performed in Center for Computational Science of CASHIPS, the ScGrid of Supercomputing Center and Computer Network Information Center of Chinese Academy of Sciences.

[1] S. Dutta, A. K. Manna, and S. K. Pati, Phys. Rev. Lett. **102**, 096601 (2009).
[2] X. Zheng, X. Wang, T. Abtew, and Z. Zeng, J. Phys. Chem. C **114**, 4190 (2010).
[3] D. D. Awschalom and M. E. Flatté, Nat. Phys. **3**, 153 (2007).
[4] X. Li and J. Yang, Natl. Sci. Rev. **3**, 365 (2016).
[5] O. L. Sanchez, D. Ovchinnikov, S. Misra, A. Allain, and A. Kis, Nano Lett. **16**, 5792 (2016).
[6] M. Ashton, D. Gluhovic, S. B. Sinnott, J. Guo, D. A. Stewart, and R. G. Hennig, Nano Lett. **17**, 5251 (2017).
[7] X. Zheng, X. Chen, L. Zhang, L. Xiao, S. Jia, Z. Zeng, and H. Guo, 2D Mater. **4**, 025013 (2017).
[8] X. Tao, L. Zhang, X. Zheng, H. Hao, X. Wang, L. Song, Z. Zeng, and H. Guo, Nanoscale **10**, 174 (2018).
[9] S.-J. Gong, C. Gong, Y.-Y. Sun, W.-Y. Tong, C.-G. Duan, J.-H. Chu, and X. Zhang, Proc. Natl. Acad. Sci. USA **115**, 8511 (2018).
[10] L. Song, S. Jin, P. Jiang, H. Hao, X. Zheng, and L. Zhang, Carbon **141**, 676 (2019).
[11] R. A. de Groot, F. M. Mueller, P. G. van Engen, and K. H. J. Buschow, Phys. Rev. Lett. **50**, 2024 (1983).

[12] J.-H. Park, E. Vescovo, H.-J. Kim, C. Kwon, R. Ramesh, and T. Venkatesan, Nature (London) **392**, 794 (1998).
[13] S. S. Mallajosyula and S. K. Pati, J. Phys. Chem. B **111**, 13877 (2007).
[14] V. V. Maslyuk, A. Bagrets, V. Meded, A. Arnold, F. Evers, M. Brandbyge, T. Bredow, and I. Mertig, Phys. Rev. Lett. **97**, 097201 (2006).
[15] Q. Wu, Y. Zhang, Q. Zhou, J. Wang, and X. C. Zeng, J. Phys. Chem. Lett. **9**, 4260 (2018).
[16] Z. Liu, J. Liu, and J. Zhao, Nano Res. **10**, 1972 (2017).
[17] X. Zhang, B. Wang, Y. Guo, Y. Zhang, Y. Chen, and J. Wang, Nanoscale Horizons **4**, 859 (2019).
[18] Y. W. Son, M. L. Cohen, and S. G. Louie, Nature (London) **444**, 347 (2006).
[19] C. Tang, L. Zhang, S. Sanvito, and A. Du, J. Mater. Chem. C **8**, 7034 (2020).
[20] E.-J. Kan, Z. Li, J. Yang, and J. G. Hou, J. Amer. Chem. Soc. **130**, 4224 (2008).
[21] T. Cao, Z. Li, and S. G. Louie, Phys. Rev. Lett. **114**, 236602 (2015).
[22] P. Jiang, L. Kang, X. Zheng, Z. Zeng, and S. Sanvito, Phys. Rev. B **102**, 195408 (2020).
[23] K. S. Novoselov, A. K. Geim, S. V. Morozov, D. Jiang, Y. Zhang, S. V. Dubonos, I. V. Grigorieva, and A. A. Firsov, Science **306**, 666 (2004).
[24] C. Zhi, Y. Bando, C. Tang, H. Kuwahara, and D. Golberg, Adv. Mater. **21**, 2889 (2009).
[25] J. Qiao, X. Kong, Z. X. Hu, F. Yang, and W. Ji, Nat. Commun. **5**, 4475 (2014).
[26] L. Li, Y. Yu, G. J. Ye, Q. Ge, X. Ou, H. Wu, D. Feng, X. H. Chen, and Y. Zhang, Nat. Nanotechnol. **9**, 372 (2014).
[27] P. Vogt, P. De Padova, C. Quaresima, J. Avila, E. Frantzeskakis, M. C. Asensio, A. Resta, B. Ealet, and G. Le Lay, Phys. Rev. Lett. **108**, 155501 (2012).
[28] D. C. Elias, R. R. Nair, T. M. G. Mohiuddin, S. V. Morozov, P. Blake, M. P. Halsall, A. C. Ferrari, D. W. Boukhvalov, M. I. Katsnelson, A. K. Geim, and K. S. Novoselov, Science **323**, 610 (2009).
[29] D. Malko, C. Neiss, F. Viñes, and A. Görling, Phys. Rev. Lett. **108**, 086804 (2012).
[30] D. D. Vaughn II, R. J. Patel, M. A. Hickner, and R. E. Schaak, J. Am. Chem. Soc. **132**, 15170 (2010).
[31] Y.-W. Son, M. L. Cohen, and S. G. Louie, Phys. Rev. Lett. **97**, 216803 (2006).
[32] O. V. Yazyev and L. Helm, Phys. Rev. B **75**, 125408 (2007).
[33] A. V. Krasheninnikov, P. O. Lehtinen, A. S. Foster, P. Pyykkö, and R. M. Nieminen, Phys. Rev. Lett. **102**, 126807 (2009).
[34] L. Seixas, A. Carvalho, and A. H. Castro Neto, Phys. Rev. B **91**, 155138 (2015).
[35] Z. Wang, C. Tang, R. Sachs, Y. Barlas, and J. Shi, Phys. Rev. Lett. **114**, 016603 (2015).
[36] A. W. Cummings, J. H. Garcia, J. Fabian, and S. Roche, Phys. Rev. Lett. **119**, 206601 (2017).
[37] R. R. Nair, M. Sepioni, I. L. Tsai, O. Lehtinen, J. Keinonen, A. V. Krasheninnikov, T. Thomson, A. K. Geim, and I. V. Grigorieva, Nat. Phys. **8**, 199 (2011).
[38] C. Gong, L. Li, Z. Li, H. Ji, A. Stern, Y. Xia, T. Cao, W. Bao, C. Wang, Y. Wang, Z. Q. Qiu, R. J. Cava, S. G. Louie, J. Xia, and X. Zhang, Nature (London) **546**, 265 (2017).
[39] C. Gong and X. Zhang, Science **363**, eaav4450 (2019).
[40] N. Sivadas, M. W. Daniels, R. H. Swendsen, S. Okamoto, and D. Xiao, Phys. Rev. B **91**, 235425 (2015).
[41] H. Wang, F. Fan, S. Zhu, and H. Wu, Europhys. Lett. **114**, 47001 (2016).
[42] B. Huang, G. Clark, E. Navarromoratalla, D. R. Klein, R. Cheng, K. L. Seyler, D. Zhong, E. Schmidgall, M. A. Mcguire, and D. H. Cobden, Nature (London) **546**, 270 (2017).
[43] F. Jun, S. Xu, W. Changzheng, P. Lele, L. Chenwen, H. Shuanglin, Y. Jinlong, and X. Yi, J. Am. Chem. Soc. **133**, 17832 (2011).
[44] H. R. Fuh, C. R. Chang, Y. K. Wang, R. F. L. Evans, R. W. Chantrell, and H. T. Jeng, Sci. Rep. **6**, 32625 (2016).
[45] M. Bonilla, S. Kolekar, Y. Ma, H. C. Diaz, V. Kalappattil, R. Das, T. Eggers, H. R. Gutierrez, M. H. Phan, and M. Batzill, Nat. Nanotechnol. **13**, 289 (2018).
[46] M. Yandong, D. Ying, G. Meng, N. Chengwang, Z. Yingtao, and H. Baibiao, ACS Nano **6**, 1695 (2012).
[47] M. Esters, R. G. Hennig, and D. C. Johnson, Phys. Rev. B **96**, 235147 (2017).
[48] W. Y. Tong and C. G. Duan, Npj Quantum Mater. **2**, 47 (2017).
[49] Y. Zhao, J.-J. Zhang, S. Yuan, and Z. Chen, Adv. Funct. Mater. **29**, 1901420 (2019).
[50] C. Gong, E. M. Kim, Y. Wang, G. Lee, and X. Zhang, Nat. Commun. **10**, 2657 (2019).
[51] G. Kresse and J. Hafner, Phys. Rev. B **47**, 558 (1993).
[52] P. E. Blöchl, Phys. Rev. B **50**, 17953 (1994).
[53] J. P. Perdew, K. Burke, and M. Ernzerhof, Phys. Rev. Lett. **77**, 3865 (1996).
[54] J. Paier, M. Marsman, K. Hummer, G. Kresse, I. C. Gerber, and J. G. Ángyán, J. Chem. Phys. **124**, 154709 (2006).
[55] S. Grimme, J. Comput. Chem. **27**, 1787 (2006).
[56] E. J. Kan, Z. Li, J. Yang, and J. G. Hou, Appl. Phys. Lett. **91**, 243116 (2007).
[57] R. Fei, W. Kang, and L. Yang, Phys. Rev. Lett. **117**, 097601 (2016).
[58] K. Chang, J. Liu, H. Lin, N. Wang, K. Zhao, A. Zhang, F. Jin, Y. Zhong, X. Hu, and W. Duan, Science **353**, 274 (2016).
[59] H. Wang and X. Qian, 2D Mater. **4**, 015042 (2017).
[60] S. Guan, C. Liu, Y. Lu, Y. Yao, and S. A. Yang, Phys. Rev. B **97**, 144104 (2018).
[61] W. Ding, J. Zhu, Z. Wang, Y. Gao, D. Xiao, Y. Gu, Z. Zhang, and W. Zhu, Nat. Commun. **8**, 14956 (2017).
[62] Z. Yu, W. Di, Y. Zhu, Y. Cho, and K. Lai, Nano Lett. **17**, 5508 (2017).
[63] C.-F. Fu, J. Sun, Q. Luo, X. Li, W. Hu, and J. Yang, Nano Lett. **18**, 6312 (2018).
[64] S. Wan, Y. Li, W. Li, X. Mao, C. Wang, C. Chen, J. Dong, A. Nie, J. Xiang, Z. Liu, W. Zhu, and H. Zeng, Adv. Funct. Mater. **29**, 1808606 (2019).
[65] A. Chandrasekaran, A. Mishra, and A. K. Singh, Nano Lett. **17**, 3290 (2017).
[66] J.-J. Zhang, L. Lin, Y. Zhang, M. Wu, B. I. Yakobson, and S. Dong, J. Am. Chem. Soc. **140**, 9768 (2018).
[67] S. Yuan, X. Luo, H. L. Chan, C. Xiao, Y. Dai, M. Xie, and J. Hao, Nat. Commun. **10**, 1775 (2019).
[68] T. Björkman, A. Gulans, A. V. Krasheninnikov, and R. M. Nieminen, Phys. Rev. Lett. **108**, 235502 (2012).

[69] See Supplemental Material at http://link.aps.org/supplemental/10.1103/PhysRevB.102.245417 for the layer-projected and spin-resolved density of states of P↑↑ and P↓↓ configurations at the HSE06 level; The atomic structure of an antiferroelectric heterostructure; The atomic structures and the corresponding spin- and layer-resolved band structures of the Sc_2CO_2/VSe_2 multiferroic heterostructures with monolayer Sc_2CO_2 contacted at one side of the VSe_2 bilayer.

[70] P. Sharma, F.-X. Xiang, D.-F. Shao, D. Zhang, E. Y. Tsymbal, A. R. Hamilton, and J. Seidel, Sci. Adv. **5**, eaax5080 (2019).

[71] N. M. Caffrey, T. Archer, I. Rungger, and S. Sanvito, Phys. Rev. Lett. **109**, 226803 (2012).

[72] N. M. Caffrey, T. Archer, I. Rungger, and S. Sanvito, Phys. Rev. B **83**, 125409 (2011).

[73] L. Kang, P. Jiang, N. Cao, H. Hao, X. Zheng, L. Zhang, and Z. Zeng, Nanoscale **11**, 16837 (2019).